

Out-of-Distribution Radar Detection with Complex VAEs: Theory, Whitening, and ANMF Fusion

Y. A. Rouzoumka, J. Pinsolle, E. Terreaux, C. Morisseau, J.-P. Ovarlez, and C. Ren

Abstract—We investigate the detection of weak complex-valued signals immersed in non-Gaussian, range-varying interference, with emphasis on maritime radar scenarios. The proposed methodology exploits a Complex-valued Variational AutoEncoder (CVAE) trained exclusively on clutter-plus-noise to perform Out-Of-Distribution detection. By operating directly on in-phase/quadrature samples, the CVAE preserves phase and Doppler structure and is assessed in two configurations: (i) using unprocessed range profiles and (ii) after local whitening, where per-range covariance estimates are obtained from neighboring profiles. Using extensive simulations together with real sea-clutter data from the CSIR maritime dataset, we benchmark performance against classical and adaptive detectors (MF, NMF, AMF-SCM, ANMF-SCM, ANMF-Tyler). In both configurations, the CVAE yields a higher detection probability P_d at matched false-alarm rate P_{fa} , with the most notable improvements observed under whitening. We further integrate the CVAE with the ANMF through a weighted log- p fusion rule at the decision level, attaining enhanced robustness in strongly non-Gaussian clutter and enabling empirically calibrated P_{fa} control under H_0 . Overall, the results demonstrate that statistical normalization combined with complex-valued generative modeling substantively improves detection in realistic sea-clutter conditions, and that the fused CVAE-ANMF scheme constitutes a competitive alternative to established model-based detectors.

Index Terms—Radar target detection, out-of-distribution detection, complex-valued neural networks, complex-valued variational autoencoder, decision-level fusion.

I. INTRODUCTION

DETECTION of weak complex-valued signals immersed in non-Gaussian interference is a central problem in statistical signal processing [1], with applications ranging from radar and sonar to wireless communications and passive sensing. In many of these modalities, the background exhibits range- or time-varying statistics, heavy tails, and residual impropriety after coherent processing, so that classical Gaussian-based detectors struggle to maintain high detection probability and reliable false-alarm rate control.

In radar target detection, the goal is to discriminate targets from complex clutter environments such as maritime or airborne scenes. Classical detectors, such as the Matched Filter (MF), the Normalized Matched Filter (NMF), and adaptive approaches including the Adaptive Matched Filter (AMF) [2], Kelly's GLRT [3], and the Adaptive Normalized Matched Filter (ANMF) [4], achieve strong performance under homogeneous complex Gaussian clutter or well-specified compound-

Y. A. Rouzoumka, E. Terreaux, C. Morisseau, and J.-P. Ovarlez are with DEMR, ONERA, Université Paris-Saclay, F-91123 Palaiseau, France (e-mail: firstname.lastname@onera.fr).

Y. A. Rouzoumka, J. Pinsolle, J.-P. Ovarlez, and C. Ren are with SONDRA, CentraleSupélec, Université Paris-Saclay, 91190 Gif-sur-Yvette, France (e-mail: firstname.lastname@centralesupelec.fr).

Gaussian models. Their effectiveness deteriorates, however, when clutter exhibits pronounced non-Gaussian characteristics combined with thermal noise, making it difficult to preserve a good P_d - P_{fa} trade-off.

Recent advances in deep learning have opened new perspectives for radar detection [5]. Variational Autoencoders (VAEs) are particularly appealing for out-of-distribution (OOD) detection [6], [7] thanks to their ability to model complex data distributions [8] and to flag deviations from learned background statistics. Beyond radar, VAEs and related deep generative models have been used for acoustic monitoring, medical imaging, and high-voltage equipment diagnostics [9]–[12]. In radar applications, a few recent works address specific short-range FMCW scenarios [13], but the systematic integration of complex VAEs into classical CFAR detection pipelines is largely unexplored.

Building on these advances, this paper introduces a complex-valued VAE (CVAE) architecture that operates directly on complex radar signals [14], thereby preserving phase information and increasing flexibility in the latent space. Complex-valued neural networks exploit joint amplitude–phase representations and have shown advantages in several signal processing tasks [15]–[18]. Here, the CVAE is used as a generative model of clutter profiles; detection relies on a complex reconstruction-error statistic, which is calibrated via per-Doppler probability-integral transforms (PIT) to enforce CFAR. We also consider a local covariance-based whitening that normalizes each Doppler profile using a neighborhood-based covariance estimate, aiming to stabilize the null distribution of CVAE scores.

To connect learned and model-based detectors, we develop a decision-level fusion strategy combining the CVAE with the classical ANMF. Both detectors are mapped to a common significance scale expressed as p -values under H_0 , and then fused via a weighted logarithmic combination reminiscent of Fisher-type p -value aggregation [19], [20]. This enables the ANMF to dominate in well-modelled Gaussian or mildly heterogeneous regimes, while the CVAE contributes robustness when clutter exhibits strong non-Gaussian behavior, with the fusion designed to preserve CFAR via empirical calibration.

In addition to extensive simulation studies with correlated Gaussian and compound-Gaussian clutter, the proposed framework is validated on real maritime radar data from the CSIR sea-clutter dataset [21], [22]. These measurements contain sea-surface returns and small targets under varying sea states and operating conditions, and have been used to study wave-height estimation and deep-learning-based sea-clutter modelling [23]–[28], providing a realistic testbed to assess the robustness of the CVAE-based detector and its fusion with

ANMF.

Contributions. This paper makes three main contributions.

(i) We formulate weak-signal detection in heterogeneous, non-Gaussian complex backgrounds as a complex-valued OOD detection problem, and we propose a CVAE architecture that operates directly on complex Doppler profiles. The latent posterior is modeled as a diagonal non-circular complex Gaussian, and we derive a closed-form KL divergence to a circular complex prior, generalizing standard real-valued and circular complex VAE formulations.

(ii) We study the impact of local covariance-based whitening as a generic statistical normalization for non-stationary complex-valued data. By comparing raw and locally whitened regimes on correlated Gaussian and compound-Gaussian clutter, as well as on real sea clutter, we show that combining local whitening with complex generative modeling can significantly sharpen detection fronts at fixed false-alarm rate compared with classical CFAR detectors.

(iii) We introduce a decision-level fusion scheme that combines a data-driven CVAE detector with a model-based ANMF through weighted log- p aggregation. Both branches are calibrated via PIT under H_0 , and the fused statistic is thresholded with an empirical CFAR-like rule. This p -value fusion framework remains valid under dependence and yields detectors that inherit robustness in heavy-tailed clutter while preserving controllable false-alarm behaviour. Although our experiments focus on maritime radar, the overall framework applies to a broad class of complex-valued sensing systems, including sonar, passive radar, and MIMO communications.

The remainder of this paper is organized as follows. Section II reviews statistical models of radar clutter and classical detection benchmarks. Section III discusses deep learning-based OOD detection and its specific challenges in radar. Section IV presents the proposed CVAE-based detector, including the complex-valued architecture, local whitening, and CVAE-ANMF fusion. Section V details the training methodology and experimental results. Section VI concludes the paper.

Notation: Matrices are denoted by bold uppercase letters and vectors by bold lowercase letters. For any matrix or vector \mathbf{A} , \mathbf{A}^T and \mathbf{A}^H denote the transpose and Hermitian (conjugate) transpose, respectively. \mathbf{I} represents the identity matrix. We denote respectively by $\mathcal{N}(\boldsymbol{\mu}, \boldsymbol{\Gamma})$ and $\mathcal{CN}(\boldsymbol{\mu}, \boldsymbol{\Gamma})$ real-valued and complex circular Gaussian distributions with mean $\boldsymbol{\mu}$ and covariance $\boldsymbol{\Gamma}$, respectively. And $\mathcal{N}(\boldsymbol{\mu}, \boldsymbol{\Gamma}, \boldsymbol{\Delta})$ denotes complex (non circular) Gaussian distribution with mean $\boldsymbol{\mu}$ and covariance $\boldsymbol{\Gamma}$ and pseudo-covariance $\boldsymbol{\Delta}$. The operator $\mathcal{T}(\rho)$ denotes a Toeplitz matrix constructed from a correlation coefficient ρ , with $\{\mathcal{T}(\rho)\}_{i,j} = \rho^{|i-j|}$. The symbols \odot and \oslash denote the Hadamard (element-wise) product and division, respectively. Similarly, $|\cdot|$, $\cdot^{\circ\alpha}$ and $\log^\circ(\cdot)$ indicate the element-wise absolute value, power to the exponent α , and logarithm of a vector. The operators $\Re\{\cdot\}$ and $\Im\{\cdot\}$ extract the real and imaginary parts of a complex argument. The operator $\text{diag}(\cdot)$ extracts the diagonal elements of a matrix.

II. STATISTICAL MODEL

A. Signal Model and Binary Hypotheses

In adaptive radar detection, we test for the presence of a complex target return $\alpha \mathbf{p} \in \mathbb{C}^m$ (with unknown complex amplitude α and known steering vector \mathbf{p} of dimension m) embedded in background clutter \mathbf{c} and independent white thermal noise $\mathbf{n} \sim \mathcal{CN}(\mathbf{0}, \sigma^2 \mathbf{I})$. The problem is cast as

$$\begin{cases} H_0 : \mathbf{z} = \mathbf{c} + \mathbf{n}, & \text{(no target),} \\ H_1 : \mathbf{z} = \alpha \mathbf{p} + \mathbf{c} + \mathbf{n}, & \text{(target present),} \end{cases} \quad (1)$$

where $\mathbf{z} \in \mathbb{C}^m$ is the received snapshot. In homogeneous environments, the clutter is modeled as circular complex Gaussian $\mathbf{c} \sim \mathcal{CN}(\mathbf{0}, \boldsymbol{\Sigma}_c)$. In heterogeneous environments a compound-Gaussian model is used, $\mathbf{c} = \sqrt{\tau} \mathbf{g}$ with $\mathbf{g} \sim \mathcal{CN}(\mathbf{0}, \boldsymbol{\Sigma}_c)$ and a positive texture parameter $\tau > 0$ describing pulse-to-pulse power fluctuations; conditionally on τ , $\mathbf{c} \sim \mathcal{CN}(\mathbf{0}, \tau \boldsymbol{\Sigma}_c)$, and we fix the power scale via $\mathbb{E}[\tau] = 1$. After whitening by the total covariance $\boldsymbol{\Sigma} = \boldsymbol{\Sigma}_c + \sigma^2 \mathbf{I}$, the signal-to-noise ratio under H_1 reads

$$\text{SNR} = |\alpha|^2 \mathbf{p}^H \boldsymbol{\Sigma}^{-1} \mathbf{p}. \quad (2)$$

B. Classical Detectors

When $\boldsymbol{\Sigma}$ is known, the MF is GLRT-optimal in Gaussian environments, and the associated detection test is expressed as:

$$\Lambda_{\text{MF}}(\mathbf{z}) = \frac{|\mathbf{p}^H \boldsymbol{\Sigma}^{-1} \mathbf{z}|^2}{\mathbf{p}^H \boldsymbol{\Sigma}^{-1} \mathbf{p}} \stackrel{H_1}{\underset{H_0}{\gtrless}} \lambda, \quad (3)$$

with Λ_{MF} exponentially distributed with unit mean under H_0 (equivalently $\Lambda_{\text{MF}} \stackrel{d}{=} \frac{1}{2} \chi_2^2$ where χ_2^2 stands for Chi-Square Distribution with two degrees of freedom), yielding $P_{fa} = e^{-\lambda}$ in the homogeneous Gaussian case. In partially homogeneous noise, where the covariance is known up to an unknown positive scale, the scale-invariant NMF [4] is defined as:

$$\Lambda_{\text{NMF}}(\mathbf{z}) = \frac{|\mathbf{p}^H \boldsymbol{\Sigma}^{-1} \mathbf{z}|^2}{(\mathbf{p}^H \boldsymbol{\Sigma}^{-1} \mathbf{p})(\mathbf{z}^H \boldsymbol{\Sigma}^{-1} \mathbf{z})} \stackrel{H_1}{\underset{H_0}{\gtrless}} \lambda. \quad (4)$$

These MF/NMF benchmarks are well understood and effective when clutter plus thermal noise remain Gaussian.

C. Adaptive Detection

In practice, $\boldsymbol{\Sigma}$ is unknown and has to be estimated from K secondary data $\{\mathbf{z}_k\}_{k=1}^K$ supposed to be target-free. In Gaussian environments, the best estimator of $\boldsymbol{\Sigma}$ is the Sample Covariance Matrix (SCM)

$$\hat{\boldsymbol{\Sigma}}_{\text{SCM}} = \frac{1}{K} \sum_{k=1}^K \mathbf{z}_k \mathbf{z}_k^H, \quad (5)$$

leading to the Adaptive Matched Filter (AMF-SCM) [2] and the Adaptive Normalized Matched Filter (ANMF-SCM) [29], obtained by inserting $\hat{\boldsymbol{\Sigma}}_{\text{SCM}}$ into (3) and (4). In compound-Gaussian (impulsive) clutter, SCM-based detectors may lose CFAR properties and degrade in P_d . Robust covariance estimation is then preferable such as M -estimators [30]–[34]

and Tyler's fixed-point (FP) estimator. The latter is defined implicitly by

$$\hat{\Sigma}_{\text{FP}} = \frac{m}{K} \sum_{k=1}^K \frac{\mathbf{z}_k \mathbf{z}_k^H}{\mathbf{z}_k^H \hat{\Sigma}_{\text{FP}}^{-1} \mathbf{z}_k}, \quad (6)$$

which is scale invariant at the snapshot level (only the normalized snapshots matter) and thus attenuates large texture fluctuations. The resulting ANMF-Tyler is obtained by replacing Σ^{-1} with $\hat{\Sigma}_{\text{FP}}^{-1}$ in (4); it is known to be effective and more stable in heavy-tailed clutter [30]–[34]. However, once additive thermal noise is present, the returns no longer follow a pure compound-Gaussian (texture \times speckle) model. Moreover, this breaks the texture invariance property of Tyler's estimator and can degrade CFAR control, even when a robust covariance estimator is used.

D. Real-World Challenges and Motivation for Learning-Based OOD

Sea clutter is markedly non-Gaussian with pronounced Range slow-time correlations; combining such clutter with thermal noise yields settings where no closed-form optimal detector is known. Classical Gaussian-based detectors (MF, AMF-SCM, ANMF-SCM) remain appropriate when the overall disturbance is Gaussian, but performance and false-alarm regulation can be severely affected otherwise. Robust extensions that plug Tyler's M-estimator in place of the SCM (ANMF-Tyler) restore CFAR behaviour under compound-Gaussian clutter, but they still rely on locally homogeneous training data and can degrade in heterogeneous clutter plus white-noise regimes. These limitations motivate data-driven alternatives. In the remainder, we leverage an out-of-distribution approach based on a CVAE trained on target-free data, and assess its use both on raw profiles and after local whitening; we further consider decision-level fusion with a model-based detector to capitalize on their complementary strengths.

III. DEEP LEARNING-BASED OOD DETECTION FOR RADAR

A. The Need for OOD Detection in Radar Processing

Classical radar detectors, such as MF, NMF, AMF, and ANMF, are derived within the Neyman-Pearson likelihood ratio framework [35] under explicit statistical models for the disturbance (clutter plus thermal noise), typically Gaussian or compound-Gaussian [2], [29]. Their optimality hinges on how well these statistical assumptions match reality. In operational settings (maritime surveillance, airborne GMTI, coastal monitoring), clutter is heterogeneous, non-stationary, and structurally rich; it exhibits long-range correlations, intermittency, and heavy tails that vary across range–Doppler cells and from scan to scan. Under such departures, even well-engineered two-step adaptive schemes suffer: the number of target-free secondary data may be insufficient or contaminated by outliers, covariance estimates become unreliable, and the false-alarm rate regulation deteriorates.

OOD detection addresses a different question than classical GLRTs: rather than testing a parametric signal-in-noise model, it asks whether a given return is statistically compatible with

the background distribution learned from target-free data. This data-driven view avoids committing to a potentially misspecified analytic clutter model and instead lets the detector adapt directly to the empirical site and sea-state-dependent statistics [7]. In other words, OOD detection provides a principled way to flag anomalies (putative targets) when explicit modeling is intractable or unreliable.

B. Deep Learning Approaches to OOD

Modern deep OOD methods fall into three broad (and complementary) families. *Reconstruction-based* approaches train autoencoders (AEs) or VAEs to reconstruct in-distribution (ID) data with small error [36], with the idea that OOD samples will incur a larger distortion because they are not well represented by the learned manifold [6], [37]. For a sample \mathbf{z} and reconstruction $\hat{\mathbf{z}}$, the reconstruction squared error $\mathcal{L}_{\text{rec}} = \|\mathbf{z} - \hat{\mathbf{z}}\|^2$ serves as an anomaly score, and thresholds are chosen to meet a prescribed P_{fa} . *Density-estimation* methods seek calibrated likelihoods under expressive generative models. Normalizing flows and related hybrids (e.g., SurVAE) learn invertible mappings that transform complex data to a tractable base density, so that likelihoods can be evaluated exactly via the change-of-variables formula [38], [39]. Energy-based objectives offer another route to likelihood-based OOD scoring [40]. *Representation-learning/contrastive* methods shape a feature space where ID clusters tightly and anomalies fall away; decisions can be formed using distances such as the Mahalanobis metric computed from ID statistics [41], [42].

In radar, reconstruction-based methods are attractive because they are unsupervised, computationally efficient at test time, and naturally compatible with stringent P_{fa} control, while avoiding the calibration challenges that plague likelihoods in very high dimensions.

C. OOD in Radar: State of the Art and Gaps

Evidence for the effectiveness of OOD has accumulated across various domains. In medical imaging, likelihood modeling in compressed latent spaces has enabled state-of-the-art anomaly localization [43]. For time series, attention-based architectures (Anomaly Transformer, TranAD) capture long-range dependencies and highlight subtle deviations [44], [45]. In radar specifically, reconstruction-based OOD detectors on short-range 60 GHz FMCW sensors have shown that autoencoder reconstruction errors (and related latent-energy scores) correlate strongly with anomalous micro-Doppler patterns [46], and our preliminary results indicate similar benefits for maritime returns [14]. However, most prior studies operate in controlled or short-range settings, leaving open the question of handling strongly correlated, heavy-tailed sea clutter with additive thermal noise, precisely where classical detectors struggle.

D. Reconstruction-Driven CVAE for Radar OOD

We adopt a complex-valued variational autoencoder [14] as the backbone of our OOD model. Training is performed exclusively on target-free radar profiles (clutter plus thermal

noise), allowing the encoder-decoder pair to learn a compact latent representation of the background. Test samples that contain a target then deviate from this manifold by inducing a larger reconstruction error $\mathcal{L}_{\text{rec}} = \|\mathbf{z} - \hat{\mathbf{z}}\|^2 = \sum_n |z_n - \hat{z}_n|^2$, which we use as our primary anomaly score in this work. In principle, one could also exploit the CVAE latent posterior as an additional signal, for instance by penalizing low-probability regions of the variational family.

Crucially, the network is complex-valued end-to-end, ingesting complex-valued data and maintaining phase coherence through complex convolutions, normalizations, and activations. This is not merely an architectural convenience: phase carries essential information for coherent integration and Doppler discrimination. Empirically and theoretically, complex-valued networks can dominate real-valued counterparts at fixed capacity in phase-sensitive modalities such as Polarimetric SAR classification [16], and recent generative designs show that complex VAEs capture structure in noisy, phase-rich signals more faithfully than real-valued surrogates [14], [17], [18]. We therefore expect CVAEs to better preserve the geometry of sea clutter and the subtle distortions induced by weak targets.

IV. COMPLEX VAE RADAR DETECTOR: ARCHITECTURE, WHITENING, AND FUSION

Parametric statistical modeling of sea clutter plus thermal noise is fragile under heterogeneity and non-Gaussianity. We therefore learn the null (H_0) distribution from a target-free corpus $\mathcal{D}_{H_0} = \{\mathbf{z}_n\}_{n \in [1, N]}$ using a Complex-valued VAE. This choice offers a pragmatic compromise for radar: the CVAE is fully unsupervised, operates natively in \mathbb{C} to preserve Doppler-phase cues, and yields a reconstruction-based anomaly score that can be calibrated to a target false-alarm rate P_{fa} . Beyond raw CVAE processing, we consider local whitening (Section IV-B) to stabilise clutter statistics, and a decision-level fusion with ANMF via weighted log- p combination (Section IV-D) to leverage complementary inductive biases across the Gaussian-to-impulsive spectrum.

A. Complex-Valued VAE Architecture

Design principle: Operating natively in \mathbb{C} preserves phase coherence and enables modeling of non-circular effects that arise after coherent processing (e.g., sea clutter with residual impropriety). Our CVAE therefore operates directly on complex-valued Doppler profiles $\mathbf{z} \in \mathbb{C}^m$, using complex convolutions, complex pooling, and complex activation functions throughout the encoder and decoder (Fig. 1). This avoids the information loss associated with ad-hoc real-imaginary stacking, and follows recent evidence that complex-valued networks can outperform real-valued ones when phase is discriminative [16]–[18].

Encoder: Given a Doppler profile $\mathbf{z} \in \mathbb{C}^m$ (raw or whitened, cf. Sec. IV-B), a stack of K complex 1D convolutional blocks maps

$$\mathbf{z} \longmapsto \mathbf{h} = \text{Conv1Dblock}(\mathbf{z}) \in \mathbb{C}^{C_K \times m_K},$$

where each block uses a complex convolution, a complex activation (modReLU or CReLU), optional complex max-pooling (implemented as max-pooling on $|\cdot|$ with complex gather), and complex batch-normalization. The terminal feature tensor \mathbf{h} is flattened and projected to three unconstrained heads

$$\boldsymbol{\mu} \in \mathbb{C}^q, \quad \tilde{\mathbf{s}} \in \mathbb{R}^q, \quad \tilde{\boldsymbol{\delta}} \in \mathbb{C}^q.$$

We write $\boldsymbol{\sigma} = \text{softplus}(\tilde{\mathbf{s}}) \in \mathbb{R}_+^q$ for the element-wise standard deviation, so that the variance in the latent distribution is $\boldsymbol{\sigma}^{\circ 2}$, and we obtain the pseudo-variance $\boldsymbol{\delta}$ from $\tilde{\boldsymbol{\delta}}$ via the constraint below. Taken together, $(\boldsymbol{\mu}, \boldsymbol{\sigma}^{\circ 2}, \boldsymbol{\delta})$ parameterize a non-circular complex Gaussian latent of dimension q ; this family strictly generalizes the circular case ($\boldsymbol{\delta} = \mathbf{0}$).

Stable constraint for the pseudo-variance: Let $(\tilde{\mathbf{s}}, \tilde{\boldsymbol{\delta}}, \boldsymbol{\mu})$ denote the unconstrained encoder outputs. We enforce numerically stable element-wise constraints via

$$\boldsymbol{\sigma} = \text{softplus}(\tilde{\mathbf{s}}), \quad \boldsymbol{\delta} = \boldsymbol{\eta} \odot \boldsymbol{\sigma}, \quad \boldsymbol{\eta} = \frac{\tilde{\boldsymbol{\delta}}}{1 + |\tilde{\boldsymbol{\delta}}|^{\circ}}, \quad (7)$$

where $|\cdot|^{\circ}$ denotes the element-wise complex modulus and \odot is the Hadamard product. The "complex softsign" mapping

$$|\boldsymbol{\eta}|^{\circ} = \frac{|\tilde{\boldsymbol{\delta}}|^{\circ}}{1 + |\tilde{\boldsymbol{\delta}}|^{\circ}} < 1$$

guarantees $|\boldsymbol{\delta}|^{\circ} < \boldsymbol{\sigma}$ by construction, while preserving the phase of $\tilde{\boldsymbol{\delta}}$. In implementation, we add a small $\varepsilon > 0$ to $\boldsymbol{\sigma}$ and to the denominators in the reparameterization for numerical robustness, but we omit ε from the formulas for clarity.

Complex reparameterization: Given $(\boldsymbol{\mu}, \boldsymbol{\sigma}, \boldsymbol{\delta})$, we sample a latent code $\mathbf{x} \in \mathbb{C}^q$ via

$$\mathbf{x} = \boldsymbol{\mu} + \mathbf{k}_r \odot \boldsymbol{\epsilon}_r + i \mathbf{k}_i \odot \boldsymbol{\epsilon}_i, \quad \boldsymbol{\epsilon}_r, \boldsymbol{\epsilon}_i \stackrel{\text{i.i.d.}}{\sim} \mathcal{N}(\mathbf{0}, \mathbf{I}), \quad (8)$$

where the element-wise scaling vectors $\mathbf{k}_r, \mathbf{k}_i \in \mathbb{R}_+^q$ are chosen so that

$$\begin{aligned} \boldsymbol{\sigma}^{\circ 2} &= \text{diag}(\mathbb{E}[(\mathbf{x} - \boldsymbol{\mu})(\mathbf{x} - \boldsymbol{\mu})^H]), \\ \boldsymbol{\delta} &= \text{diag}(\mathbb{E}[(\mathbf{x} - \boldsymbol{\mu})(\mathbf{x} - \boldsymbol{\mu})^{\top}]). \end{aligned}$$

Matching second-order moments leads to the element-wise mapping (cf. [47])

$$\begin{cases} \mathbf{k}_r = \frac{1}{\sqrt{2}} \frac{\boldsymbol{\sigma} + \boldsymbol{\delta}}{(\boldsymbol{\sigma} + \Re(\boldsymbol{\delta}))^{\circ 1/2}}, \\ \mathbf{k}_i = \frac{1}{\sqrt{2}} \frac{(\boldsymbol{\sigma}^{\circ 2} - (|\boldsymbol{\delta}|^{\circ})^{\circ 2})^{\circ 1/2}}{(\boldsymbol{\sigma} + \Re(\boldsymbol{\delta}))^{\circ 1/2}}, \end{cases} \quad (9)$$

where all powers and absolute values are taken element-wise. In code, we add a small ε inside the square roots and denominators of (9) to avoid numerical issues when the denominator is small.

Decoder and objective: The decoder mirrors the encoder: a fully-connected layer reshapes $\mathbf{x} \in \mathbb{C}^q$ into feature maps, then a stack of complex 1D transposed convolutions and complex activations upsamples back to $\hat{\mathbf{z}} \in \mathbb{C}^m$. Reconstruction in the complex domain preserves the phase-sensitive Doppler structure exploited by the detectors.

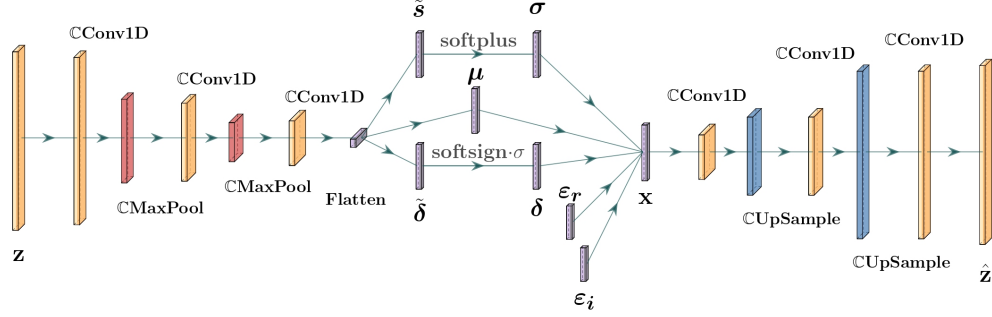


Fig. 1. Complex-valued VAE architecture used in this work. The encoder applies complex 1D convolutions and pooling to a Doppler profile $\mathbf{z} \in \mathbb{C}^m$ and produces three heads $(\boldsymbol{\mu}, \tilde{s}, \tilde{\delta})$. The unconstrained outputs \tilde{s} and $\tilde{\delta}$ are mapped to the variance σ and pseudo-variance δ via a softplus and a complex softsign- σ transform. A complex reparameterization with two real noise vectors $\boldsymbol{\varepsilon}_r, \boldsymbol{\varepsilon}_i$ yields latent samples $\mathbf{x} \in \mathbb{C}^q$, which are decoded back to $\hat{\mathbf{z}} \in \mathbb{C}^m$ via complex transposed convolutions and upsampling.

Training minimizes over a complex-domain the well-known ELBO (Evidence Lower BOund) [48], which leads to the following loss function:

$$\mathcal{L}_{\text{CVAE}} = \underbrace{\|\mathbf{z} - \hat{\mathbf{z}}\|^2}_{\mathcal{L}_{\text{rec}}} + \beta \underbrace{\mathcal{D}_{\text{KL}}(q(\mathbf{x}|\mathbf{z}) \| p(\mathbf{x}))}_{\mathcal{L}_{\text{KL}}}, \quad (10)$$

where \mathcal{L}_{rec} is the reconstruction term and $p(\mathbf{x}) = \mathcal{CN}(\mathbf{0}, \mathbf{I}_q)$ is a standard circular complex prior, and where the rate-distortion balance parameter $\beta > 0$ controls the anomaly sensitivity of the detector through the Kullback-Liebler (KL) divergence between the distribution p and the posterior distribution $q(\mathbf{x}|\mathbf{z})$ defined here as a diagonal non-circular complex Gaussian:

$$q(\mathbf{x}|\mathbf{z}) = \mathcal{CN}(\boldsymbol{\mu}, \boldsymbol{\Sigma}, \boldsymbol{\Delta}), \quad \boldsymbol{\Sigma} = \text{Diag}(\boldsymbol{\sigma}^{\circ 2}), \quad \boldsymbol{\Delta} = \text{Diag}(\boldsymbol{\delta}),$$

with variance $\boldsymbol{\sigma}^{\circ 2}$ and pseudo-variance $\boldsymbol{\delta}$ parameterized as in (7). For this family, the KL divergence between $q(\mathbf{x}|\mathbf{z})$ and the circular prior admits the closed-form

$$\mathcal{D}_{\text{KL}} = \boldsymbol{\mu}^H \boldsymbol{\mu} + \mathbf{1}_q^\top \left(\boldsymbol{\sigma} - \frac{1}{2} \log^\circ (\boldsymbol{\sigma}^{\circ 2} - (|\boldsymbol{\delta}|^\circ)^{\circ 2}) \right), \quad (11)$$

where $\mathbf{1}_q$ is the q -dimensional vector of ones. This expression reduces to the standard (complex circular) VAE KL when $\boldsymbol{\delta} = \mathbf{0}$ and, when further restricted to \mathbb{R} , to the usual real-valued VAE KL. A derivation based on the scalar complex Gaussian KL and the effective variance formalism [47], [49], [50] is provided in the online supplementary material.

B. Data Preprocessing and Local Whitening

We evaluate all detectors both on raw and on locally whitened data streams. Let $\mathbf{Y} \in \mathbb{C}^{N_{\text{ranges}} \times N_{\text{pulses}}}$ denote the complex range-pulse matrix over the Doppler integration time, where N_{ranges} is the number of range gates and N_{pulses} the number of integrated pulses. For each range index r and short-time index p , we extract a slow-time snapshot

$$\mathbf{y}_{r,p} = \mathbf{Y}(r, p : p + m) \in \mathbb{C}^m,$$

of fixed length m (matching the CVAE input dimension).

Around each Cell Under Test at range index r , we define a local neighborhood \mathcal{N}_r of N_{adj} adjacent range gates (excluding r itself). From all available slow-time snapshots in this neighborhood, we build a local data matrix

$$\mathbf{Y}_{\mathcal{N}_r} \in \mathbb{C}^{m \times K_r},$$

by stacking as columns the vectors $\mathbf{y}_{r',p}$ for $r' \in \mathcal{N}_r$ and all relevant snapshot indices p . Here K_r denotes the total number of such local snapshots.

The local sample covariance at range r is then

$$\hat{\mathbf{R}}_{\mathcal{N}_r} = \frac{1}{K_r} \mathbf{Y}_{\mathcal{N}_r} \mathbf{Y}_{\mathcal{N}_r}^H \in \mathbb{C}^{m \times m}, \quad (12)$$

which we regularize (in a Ledoit-Wolf way [51]) by a small ridge term to avoid ill-conditioning:

$$\hat{\mathbf{R}}_{\text{reg}} = \hat{\mathbf{R}}_{\mathcal{N}_r} + \varepsilon_{\text{ridge}} \frac{\text{tr}(\hat{\mathbf{R}}_{\mathcal{N}_r})}{m} \mathbf{I}_m, \quad \varepsilon_{\text{ridge}} > 0. \quad (13)$$

Each slow-time snapshot at range r is whitened as

$$\mathbf{y}_{r,p}^w = \hat{\mathbf{R}}_{\text{reg}}^{-\frac{1}{2}} \mathbf{y}_{r,p}. \quad (14)$$

Finally, the corresponding one-dimensional Doppler profile is obtained by

$$\mathbf{z}_{r,p}^w = \text{DFT}(\mathbf{y}_{r,p}^w) \in \mathbb{C}^m. \quad (15)$$

where $\text{DFT}(\mathbf{v})$ stands for Discrete Fourier Transform of the vector \mathbf{v} .

This local CFAR-like normalization homogenizes the clutter power and reduces correlation in slow time, while the subsequent unitary DFT preserves the whitening in the Doppler domain and coherent target returns.

C. Detection Statistic and P_{fa} Regulation

Given a trained CVAE, the primary anomaly score is the complex reconstruction error

$$s^{\text{CVAE}}(\mathbf{z}) = \|\mathbf{z} - \hat{\mathbf{z}}\|^2 = \sum_n |z_n - \hat{z}_n|^2. \quad (16)$$

We calibrate a threshold on a *disjoint* H_0 evaluation set to meet a target false-alarm rate:

$$s^{\text{CVAE}}(\mathbf{z}) \gtrless_{H_0}^{H_1} \lambda_{\text{CVAE}}, \quad \lambda_{\text{CVAE}} = F_{s^{\text{CVAE}}|H_0}^{-1}(1 - P_{fa}), \quad (17)$$

and we repeat the calibration for the raw and whitened streams. This empirical CFAR-like setting avoids parametric assumptions on the tail of s^{CVAE} under H_0 . From a theoretical detection perspective, the CVAE reconstruction score $s^{\text{CVAE}}(\mathbf{z})$

Algorithm 1 Local Whitening Before Doppler Processing

Require: Complex range-pulse matrix $\mathbf{Y} \in \mathbb{C}^{N_{\text{ranges}} \times N_{\text{pulses}}}$,
adjacency parameter N_{adj} , ridge parameter $\varepsilon_{\text{ridge}} > 0$
Ensure: Whitened Doppler profiles $\{\mathbf{z}_{r,p}^w\}$ (assembled into \mathbf{Z}^w)

- 1: Segment \mathbf{Y} into slow-time snapshots $\{\mathbf{y}_{r,p} \in \mathbb{C}^m\}$ for all ranges r and snapshot indices p (m = snapshot length).
- 2: **for** each range index $r = 1, \dots, N_{\text{ranges}}$ **do**
- 3: Define the neighborhood \mathcal{N}_r of N_{adj} adjacent ranges (excluding r).
- 4: Form the local data matrix $\mathbf{Y}_{\mathcal{N}_r} = [\mathbf{y}_{r',p}]_{r' \in \mathcal{N}_r, p \in \mathbb{C}^{m \times K_r}}$, where K_r is the number of local reference snapshots.
- 5: Compute the sample covariance $\hat{\mathbf{R}}_r = \frac{1}{K_r} \mathbf{Y}_{\mathcal{N}_r} \mathbf{Y}_{\mathcal{N}_r}^H$.
- 6: Regularize: $\hat{\mathbf{R}}_{\text{reg}} = \hat{\mathbf{R}}_r + \varepsilon_{\text{ridge}} \frac{\text{tr}(\hat{\mathbf{R}}_r)}{m} \mathbf{I}_m$.
- 7: **for** each snapshot index p **do**
- 8: Whiten slow-time snapshot: $\mathbf{y}_{r,p}^w = \hat{\mathbf{R}}_{\text{reg}}^{-1/2} \mathbf{y}_{r,p}$.
- 9: Compute whitened Doppler profile: $\mathbf{z}_{r,p}^w = \text{DFT}(\mathbf{y}_{r,p}^w)$.
- 10: **end for**
- 11: **end for**
- 12: Assemble the whitened Doppler profiles $\{\mathbf{z}_{r,p}^w\}$ back into a matrix \mathbf{Z}^w .
- 13: **return** \mathbf{Z}^w .

can be viewed as a learned, non-linear surrogate for the log-likelihood ratio between a flexible alternative model and the background model implicitly defined by the decoder. Thresholding s^{CVAE} at fixed P_{fa} therefore provides an empirical approximation to a Neyman-Pearson test [35] in regimes where explicit clutter likelihoods are not tractable.

D. Weighted Log- p Fusion with ANMF

To exploit complementarity between the data-driven CVAE and the model-based ANMF, we map each detector score onto a common significance scale via the Probability Integral Transform (PIT) under H_0 [52]–[54]. For each Doppler bin b , we build Empirical Cumulative Distribution Functions (ECDFs) \hat{F}_b^{CVAE} and \hat{F}_b^{ANMF} from H_0 evaluation data and compute

$$p_b^{\text{CVAE}} = 1 - \hat{F}_b^{\text{CVAE}}(s^{\text{CVAE}}), \quad p_b^{\text{ANMF}} = 1 - \hat{F}_b^{\text{ANMF}}(s^{\text{ANMF}}).$$

In the ideal case, where \hat{F}_b coincides with the true null Cumulative Distribution Functions (CDF), the PIT variables are exactly uniform on $(0, 1)$ under H_0 , so that p_b^{CVAE} and p_b^{ANMF} are valid p -values, and any per-bin quantile thresholding yields an exact CFAR detector. Using the empirical CDF \hat{F}_{H_0} built from N_b background snapshots, the CFAR deviation is uniformly controlled at rate $O(N_b^{-1/2})$ by the classical Dvoretzky-Kiefer-Wolfowitz concentration inequality for empirical CDFs [55]; a short derivation is given in the online supplementary material.

We then define the fusion score as a directed weighted Fisher/Lancaster combination [19], [20]:

$$S_b^* = -(w_b \log p_b^{\text{ANMF}} + (1 - w_b) \log p_b^{\text{CVAE}}), \quad w_b \in [0, 1]. \quad (18)$$

where the weights w_b are chosen arbitrarily. In the following, we propose a strategy to recover CFAR by re-estimating the null CDF of S_b^* from clutter-only data.

Choice of weights w_b : We consider two practical options: (i) a data-driven schedule based on the CVAE's null p -values; (ii) a prior shaping that emphasizes ANMF around low Doppler.

For the data-driven schedule, we define the weights w_b as:

$$w_b = \frac{1}{1 + \exp\left(-\frac{\bar{p}_b - \mu_p}{\sigma_p}\right)}, \quad (19)$$

where $\bar{p}_b = \frac{1}{N_b} \sum_{i=1}^{N_b} p_{b,i}^{\text{CVAE}}$, $\mu_p = \frac{1}{m} \sum_{b=1}^m \bar{p}_b$, and where $\sigma_p = \frac{1}{m} \sum_{b=1}^m (\mu_p - p_b)^2$.

This upweights ANMF in regions where the CVAE appears less discriminative under H_0 , without requiring any prior on b .

When low Doppler is known to be challenging, we also consider a Gaussian prior centered at a reference bin b_0 :

$$w_b = \exp\left(-\frac{1}{2} \left(\frac{d(b, b_0)}{\sigma_0}\right)^2\right), \quad (20)$$

where $d(b, b_0)$ defines the distance between b and b_0 Doppler bins and where σ_0 is the Doppler parameter width. In our experiments, we set b_0 to the zero-Doppler bin, which concentrates the most difficult clutter/target discrimination cases.

Empirical CFAR calibration under dependence: Since CVAE and ANMF may be dependent, we estimate the null law of S_b^* empirically using paired H_0 samples (same index for p_b^{CVAE} and p_b^{ANMF}), and set bin-wise thresholds via a finite-sample quantile:

$$\lambda_{\text{fusion}}(b) = F_{S_b^* | H_0}^{-1}(1 - P_{fa}). \quad (21)$$

V. RESULTS AND SIMULATIONS

We evaluate the proposed CVAE-based detector and its decision-level fusion with ANMF (Section IV-D) against MF, NMF, AMF-SCM, and ANMF-Tyler on both simulated noise environments and real sea clutter. In all experiments, we report the probability of detection P_d as a function of the signal-to-noise ratio (SNR) at a fixed false-alarm probability $P_{fa} = 10^{-2}$, and we provide results both before and after local whitening (Section IV-B).

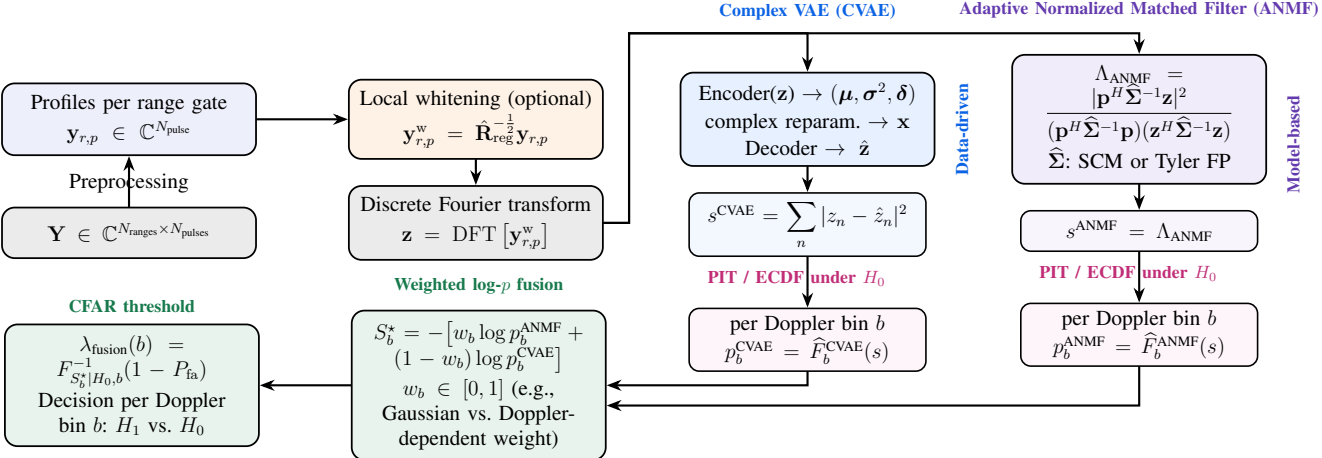


Fig. 2. Two-branch detection pipeline combining data-driven and model-based approaches.

A. Experimental Setups

1) *Signal and noise characteristics*: The complex target echo is modeled as

$$\alpha = \sqrt{\frac{\text{SNR}}{m}} e^{2j\pi\phi}, \quad \phi \sim \mathcal{U}([0, 1]), \quad (22)$$

with Doppler steering vector

$$\mathbf{p} = \left(1, e^{2j\pi d/m}, \dots, e^{2j\pi d(m-1)/m}\right)^T, \quad (23)$$

for $m = 16$ Doppler bins, where $d \in \{0, \dots, m-1\}$ denotes the $(d+1)$ th bin.

The disturbance environments considered in the simulation are:

- **Correlated Gaussian Noise (cGN):** $\mathbf{c} \sim \mathcal{CN}(\mathbf{0}, \Sigma_c)$, where $\Sigma_c = \mathcal{T}(\rho)$ is a Toeplitz matrix with correlation coefficient $\rho = 0.5$.
- **Correlated Compound Gaussian Noise (cCGN):** $\mathbf{z} = \sqrt{\tau} \mathbf{c}$, with $\mathbf{c} \sim \mathcal{CN}(\mathbf{0}, \Sigma_c)$ and τ a Gamma-distributed texture, $\tau \sim \Gamma(\mu, 1/\mu)$ with $\mu = 1$, representing heavy-tailed correlated clutter.
- **Additive White Gaussian Noise (AWGN):** $\mathbf{n} \sim \mathcal{CN}(\mathbf{0}, \sigma_n^2 \mathbf{I})$, modelling thermal noise with power σ_n^2 .

Then, we consider mixed environments where the thermal noise is added to the clutter component. In the Gaussian Noise case (cGN+AWGN), the disturbance is given by $\mathbf{z} = \mathbf{c} + \mathbf{n}$, while in the Compound Gaussian case (cCGN+AWGN) we use $\mathbf{z} = \sqrt{\tau} \mathbf{c} + \mathbf{n}$.

For adaptive detectors, the covariance matrix is estimated using the SCM or Tyler's estimator with $K = 2m$ secondary data.

2) *CSIR sea clutter data*: We validate the proposed approach on two CSIR maritime X-band recordings (South African coast). For concision, we retain the fields most relevant to detection and reproducibility. Table I summarizes radar and processing metadata.

TABLE I
CSIR METADATA (INSTRUMENT/RADAR/PROCESSING).

	CFA16-002	CFA16-008
Type	Sea clutter	Sea clutter
Transmitter frequency	6.9 GHz	6.9 GHz
Pulse Repetition Frequency	5 kHz	5 kHz
Range resolution	15 m	15 m
Range extent	1440 m (96 gates)	1440 m (96 gates)

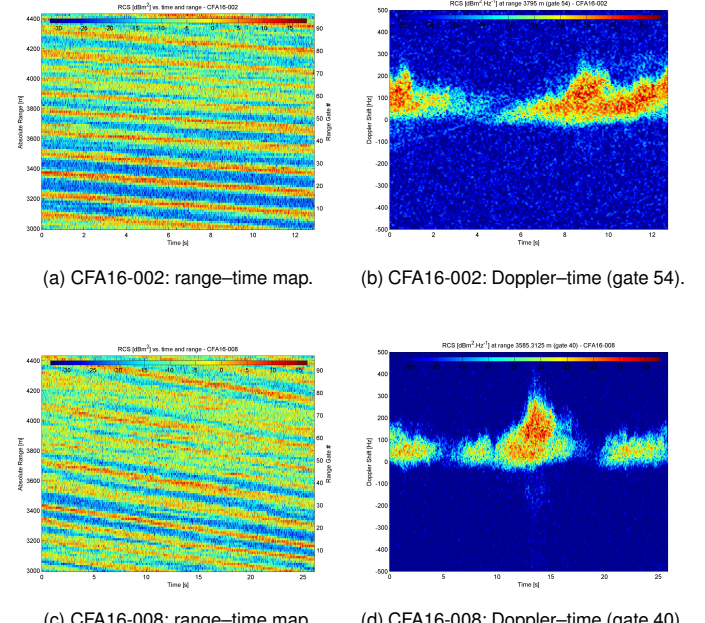


Fig. 3. CSIR sea-clutter datasets used in Section V. Left: range-time maps (96 range gates, 15 m resolution). Right: Doppler-time spectrograms at the gates used for detection analysis. Same color scale across panels.

B. Simulated Data: Zero-Doppler ($d = 0$) Curves

Figure 4 reports P_d vs. SNR at Doppler bin $d = 0$ under cGN+AWGN, cCGN, and cCGN+AWGN. Each panel compares MF/NMF baselines, AMF-SCM or ANMF-Tyler, and the CVAE detector (raw, locally whitened, and oracle-whitened when applicable). Oracle-whitened refers to the same

Algorithm 2 CVAE-ANMF Detection with Whitening and Log- p Fusion

Require: Training set $\mathcal{D}_{\text{train}}$ (clutter, H_0), evaluation set $\mathcal{D}_{\text{eval}}$

 (clutter, H_0), test set $\mathcal{D}_{\text{test}}$, target false-alarm level P_{fa}
Ensure: Detection decisions on $\mathcal{D}_{\text{test}}$ (per Doppler bin b)

 1: **Preprocessing (pre-whitening before Doppler):** For each CPI in $\mathcal{D}_{\text{train}}$, $\mathcal{D}_{\text{eval}}$, and $\mathcal{D}_{\text{test}}$, apply the segmentation and local whitening of Alg. 1:

- extract slow-time snapshots $\mathbf{y}_{r,p} \in \mathbb{C}^m$,
- estimate a local covariance $\hat{\mathbf{R}}_{\mathcal{N}_r}$ from adjacent ranges and form a whitening operator $\hat{\mathbf{R}}_{\text{reg}}^{-1/2}$,
- whiten $\mathbf{y}_{r,p}^w = \hat{\mathbf{R}}_{\text{reg}}^{-1/2} \mathbf{y}_{r,p}$,
- compute the Doppler profiles $\mathbf{z}_{r,p}^w = \text{DFT}(\mathbf{y}_{r,p}^w)$.

 Denote by $\mathcal{Z}_{\text{train}}$, $\mathcal{Z}_{\text{eval}}$, and $\mathcal{Z}_{\text{test}}$ the resulting collections of (optionally) whitened Doppler profiles $\mathbf{z}_{r,p}^w$. For notational simplicity, we write \mathbf{z} for such profiles in the sequel.

 2: **CVAE training:** Train the complex VAE on $\mathcal{Z}_{\text{train}}$ under H_0 using the β -ELBO objective in (10).

 3: **Score computation on $\mathcal{Z}_{\text{eval}}$:** For each Doppler bin b and each evaluation profile $\mathbf{z} \in \mathcal{Z}_{\text{eval}}$, compute the CVAE reconstruction score $s^{\text{CVAE}}(\mathbf{z})$ as in (16) and the ANMF statistic $s^{\text{ANMF}}(\mathbf{z})$ (Sec. II).

 4: **Null calibration and fusion thresholds:** For each bin b :

- 1) Build empirical CDFs \hat{F}_b^{CVAE} and \hat{F}_b^{ANMF} from the H_0 scores on $\mathcal{Z}_{\text{eval}}$.
- 2) Map scores to p -values via the PIT: $p_b^{\text{CVAE}} = 1 - \hat{F}_b^{\text{CVAE}}(s^{\text{CVAE}})$, $p_b^{\text{ANMF}} = 1 - \hat{F}_b^{\text{ANMF}}(s^{\text{ANMF}})$.
- 3) Choose weights w_b (e.g., sigmoid schedule or Gaussian prior) and form the fused statistic S_b^* as in (18) from paired p -values ($p_b^{\text{CVAE}}, p_b^{\text{ANMF}}$).
- 4) Estimate the null CDF $F_{S_b^*|H_0,b}$ from the fused H_0 samples and set the fusion threshold $\lambda_{\text{fusion}}(b) = F_{S_b^*|H_0,b}^{-1}(1 - P_{\text{fa}})$.

 5: **Testing on $\mathcal{Z}_{\text{test}}$:** For each test profile $\mathbf{z} \in \mathcal{Z}_{\text{test}}$ and each Doppler bin b :

- 1) Compute $s^{\text{CVAE}}(\mathbf{z})$ and $s^{\text{ANMF}}(\mathbf{z})$.
- 2) Map to p -values using the precomputed CDFs: $p_b^{\text{CVAE}}, p_b^{\text{ANMF}}$.
- 3) Form S_b^* via (18) and decide

$$\text{declare } H_1 \text{ at bin } b \iff S_b^* \geq \lambda_{\text{fusion}}(b).$$

 6: **return** Decisions $\{H_0, H_1\}$ on all Doppler bins of $\mathcal{Z}_{\text{test}}$.

process as local whitening, but uses the true covariance matrix, which is only available in simulation.

In the nearly Gaussian cGN+AWGN case (Fig. 4(a)), the MF curve is an upper bound and both the raw and oracle-whitened CVAE closely match it, while NMF and locally whitened CVAE incur a small rightward shift and AMF-SCM/ANMF-Tyler show the largest SNR loss from covariance estimation. Under heavy-tailed cCGN (Fig. 4(b)), NMF remains a strong benchmark but ANMF-Tyler degrades, whereas all CVAE variants yield steeper P_d -SNR transitions and approach NMF at medium-to-high SNR. When white noise is added (cCGN+AWGN, Fig. 4(c)), all detectors benefit from

partial “Gaussianization”, but the CVAE achieves a given P_d at noticeably lower SNR than ANMF-Tyler; oracle whitening gives a slight additional gain, whereas local whitening has limited impact. These trends are summarized in Table II.

C. Simulated Data: Full Doppler P_d -SNR Maps

We now examine P_d as a joint function of SNR and Doppler bin for the simulated clutter models. Each heatmap shows AMF-SCM, ANMF-Tyler, and the CVAE variants over all $m = 16$ Doppler bins.

For cGN+AWGN (Fig. 5), all detectors exhibit nearly vertical detection fronts, confirming Doppler-invariant homogeneous clutter once correlation is handled; the oracle CVAE aligns with the MF/NMF benchmark, and the raw CVAE reproduces this behavior, while local whitening and adaptive covariance estimation shift the fronts slightly to higher SNR. In cCGN (Fig. 6), AMF-SCM is clearly degraded and Doppler-dependent, ANMF-Tyler partly restores robustness but still requires several extra dB, and the raw/oracle CVAE yield the leftmost and sharpest fronts, nearly Doppler-invariant. Adding white noise (cCGN+AWGN, Fig. 7) moves all fronts left and reduces Doppler dependence; AMF-SCM remains suboptimal, ANMF-Tyler stays behind the CVAE by roughly 2–3 dB over most bins, and local whitening has a limited smoothing effect. These qualitative rankings are consolidated in Table II.

D. CSIR Data: Zero-Doppler ($d = 0$) Curves

For the CSIR sea clutter, we report P_d vs. SNR at $d = 0$ for both scenes (CFA16-002 and CFA16-008) and for both raw and locally whitened preprocessing. The same CFAR calibration ($P_{fa} = 10^{-2}$) is applied to all detectors.

On CFA16-002 without whitening (Fig. 8(a)), ANMF-Tyler is the strongest baseline and outperforms AMF-SCM by about 1–1.5 dB, while the raw CVAE is clearly miscalibrated and reaches a given P_d only at higher SNR, so that CVAE+ANMF essentially reduces to ANMF. After local whitening (Fig. 8(b)), the CVAE becomes more complementary: although not dominant on its own, it improves in the medium-to-high P_d range, and the fusion yields a leftmost curve, typically saving about 1–2 dB around $P_d \approx 0.8$ compared with ANMF-Tyler.

For CFA16-008, the raw case (Fig. 8(c)) shows a similar hierarchy: ANMF-Tyler and AMF-SCM behave as on CFA16-002, whereas the raw CVAE remains weak at low-to-moderate SNR. The sigmoid fusion can then slightly degrade performance with respect to pure ANMF, while the b_0 -prior fusion tends to track ANMF more closely. Once local whitening is applied (Fig. 8(d)), the CVAE strengthens markedly, with a steeper transition in SNR and performance comparable to AMF-SCM; the fusion rules can fully exploit this complementarity, and the sigmoid-based combination becomes the best overall curve, with a gain of roughly 0.5–1 dB at intermediate P_d . Overall, these zero-Doppler results indicate that whitening acts primarily as an enabler for the CVAE, after which CVAE+ANMF can improve upon classical adaptive detectors at fixed CFAR.

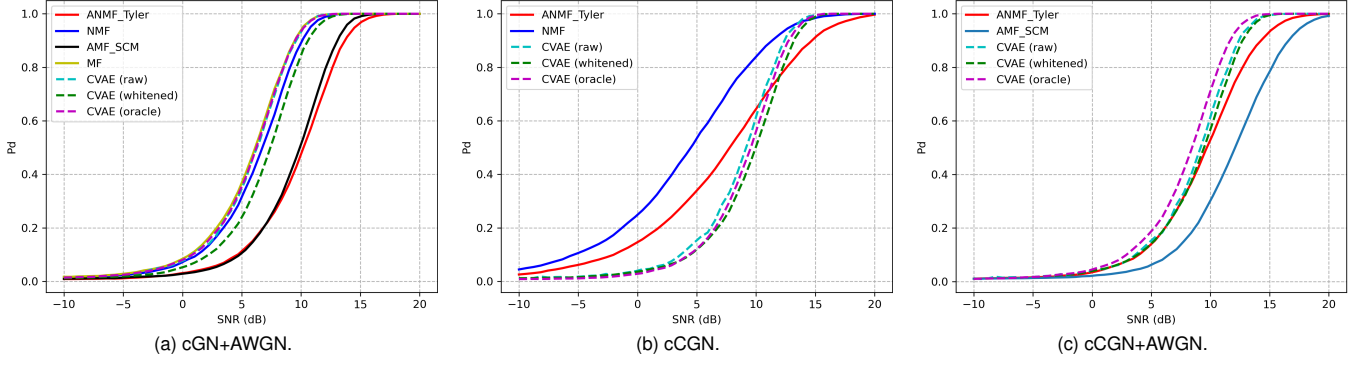


Fig. 4. P_d vs. SNR at $d = 0$ under different simulated noise models ($P_{fa} = 10^{-2}$, $\rho = 0.5$, $\mu = 1$, $m = 16$, $K = 32$).

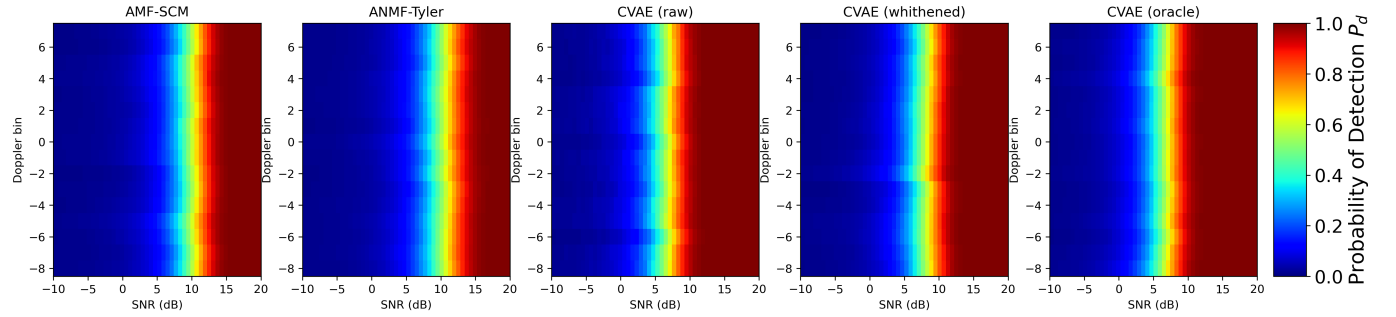


Fig. 5. P_d -SNR-Doppler maps for the cGN+AWGN setting ($P_{fa} = 10^{-2}$). Left to right: AMF-SCM, ANMF-Tyler, CVAE (raw), CVAE (whitened), and oracle CVAE whitening.

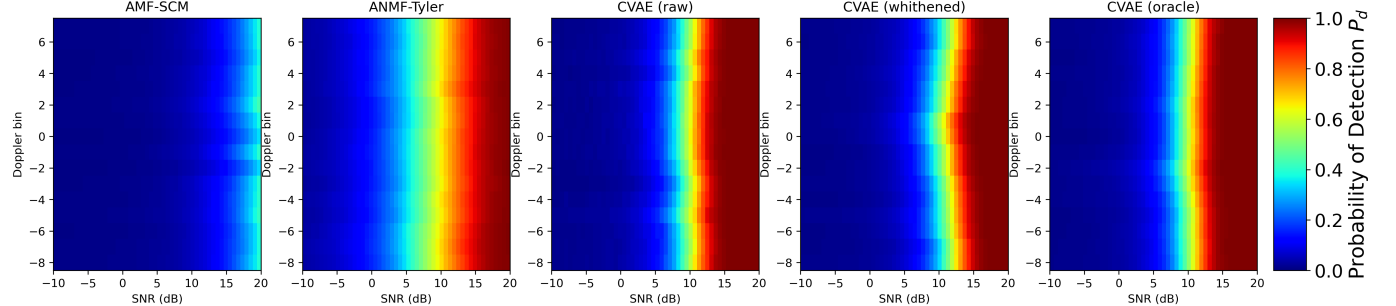


Fig. 6. P_d -SNR-Doppler maps for the cCGN setting (compound clutter, no white noise).

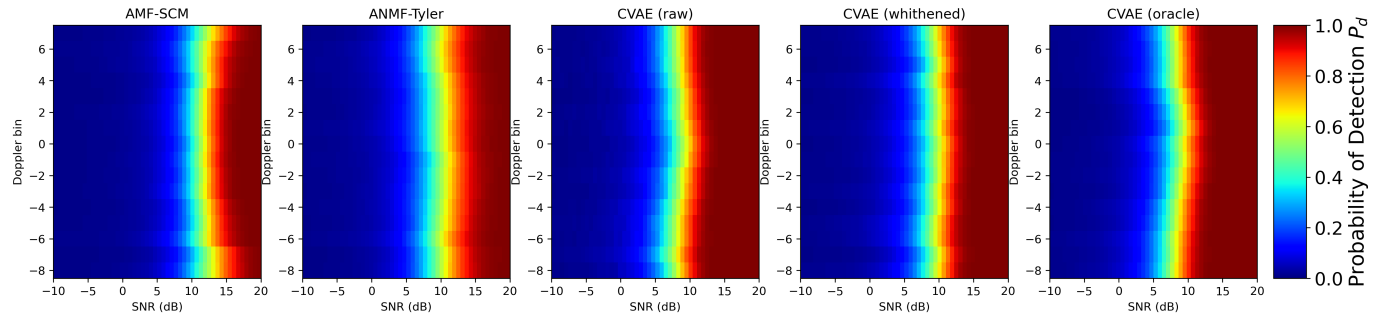


Fig. 7. P_d -SNR-Doppler maps for the cCGN+AWGN setting.

E. CSIR Data: Full Doppler P_d -SNR Maps

We now examine P_d as a function of SNR and Doppler bin for the real sea clutter. We report separate maps for each

scene (CFA16-002 and CFA16-008) and for raw vs. locally whitened processing. Each figure stacks AMF-SCM, ANMF-Tyler, CVAE, and the proposed fusion.

TABLE II

QUALITATIVE RANKING OF DETECTORS ON SIMULATED CLUTTER ($P_{fa} = 10^{-2}$). SYMBOLS: “++” BEST OR NEAR-OPTIMAL, “+” GOOD, “0” MODERATE, “-” CLEARLY SUBOPTIMAL IN TERMS OF P_d -SNR (CONSISTENT WITH BOTH THE $d=0$ CURVES AND THE FULL DOPPLER MAPS).

Scenario	MF/NMF	AMF-SCM	ANMF-Tyler	CVAE (raw)	CVAE (loc. white)	CVAE (oracle)
cGN+AWGN	++	0	0	++	+	++
cCGN	++	-	0	+	+	+
cCGN+AWGN	-	-	0	++	+	++

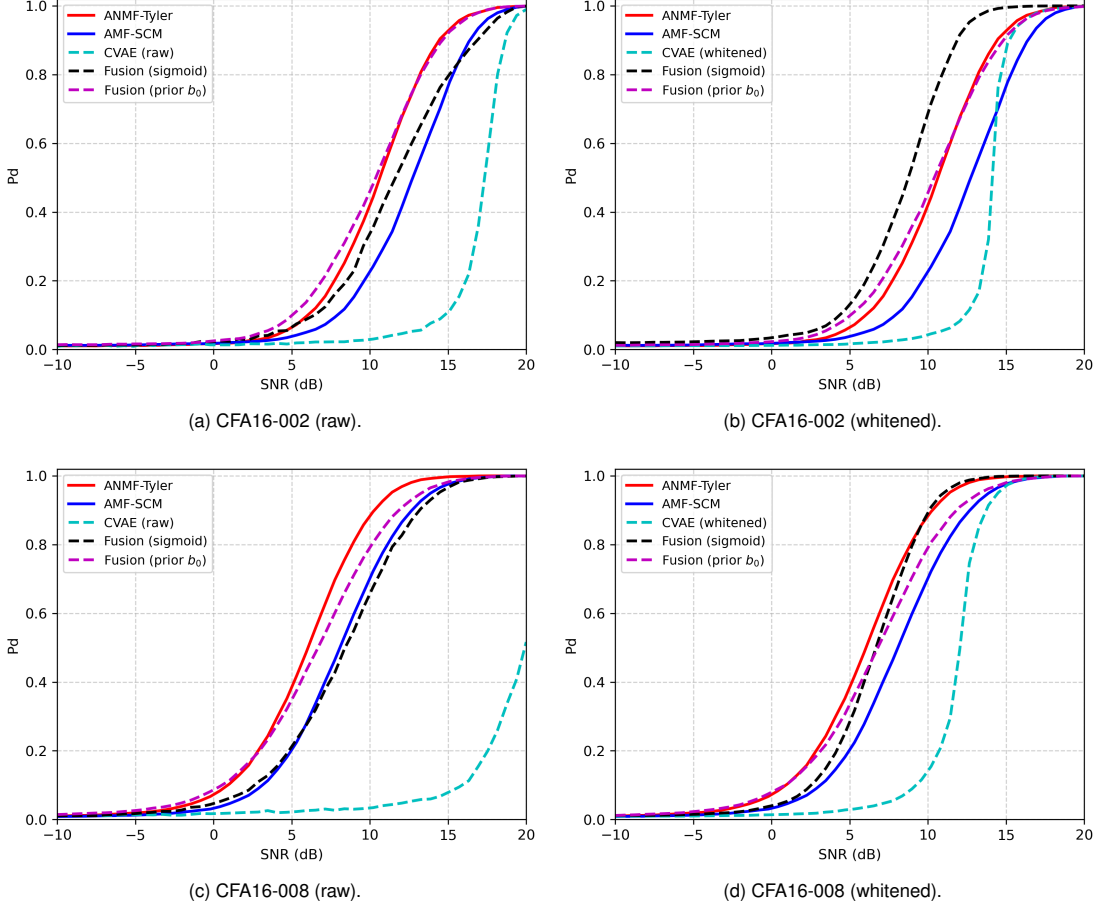


Fig. 8. P_d vs. SNR at $d=0$ for CFA16-002 and CFA16-008 ($P_{fa} = 10^{-2}$). Curves compare AMF-SCM, ANMF-Tyler, CVAE (raw/whitened), and the proposed CVAE+ANMF fusion (mean- p sigmoid; the b_0 -prior variant is reported in the appendix).

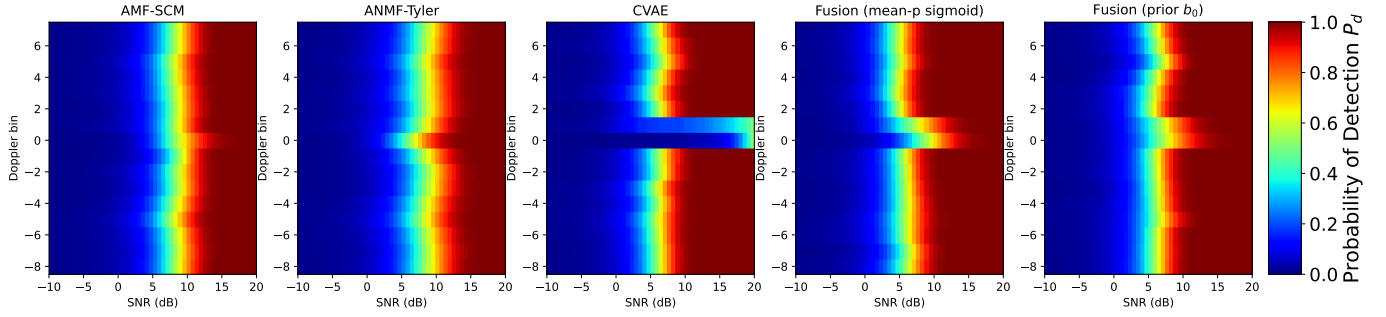
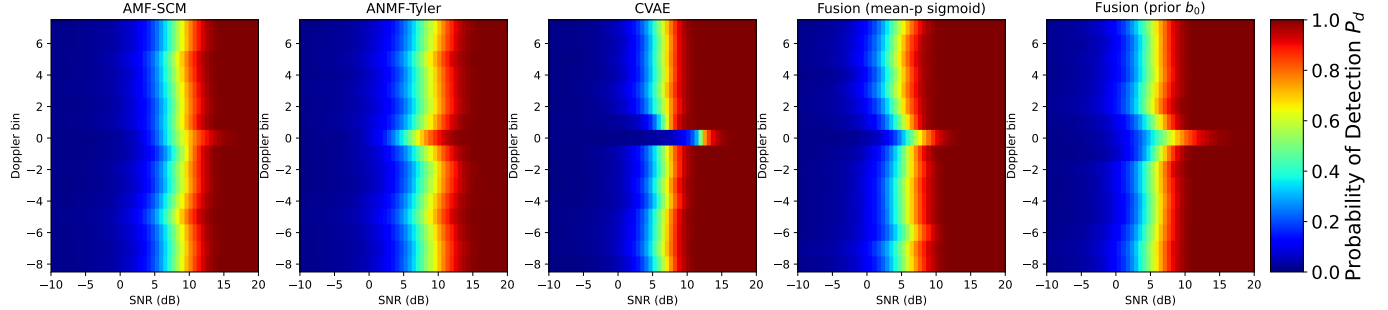
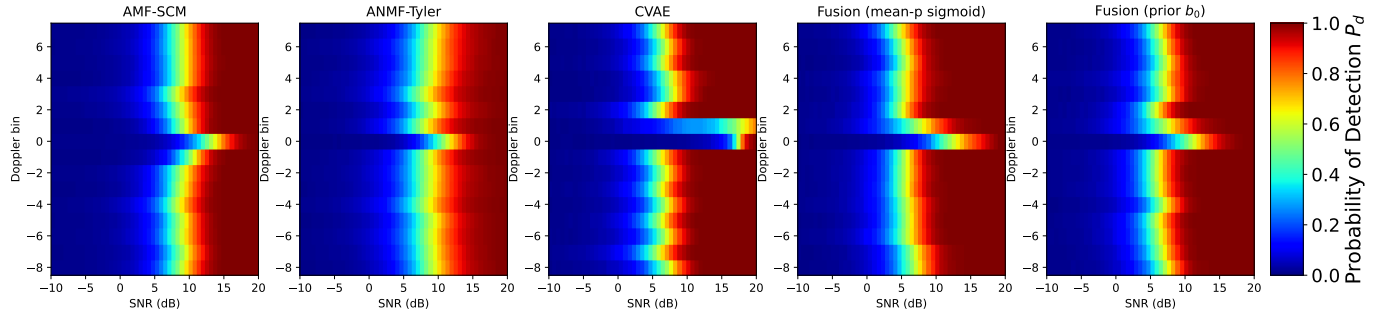
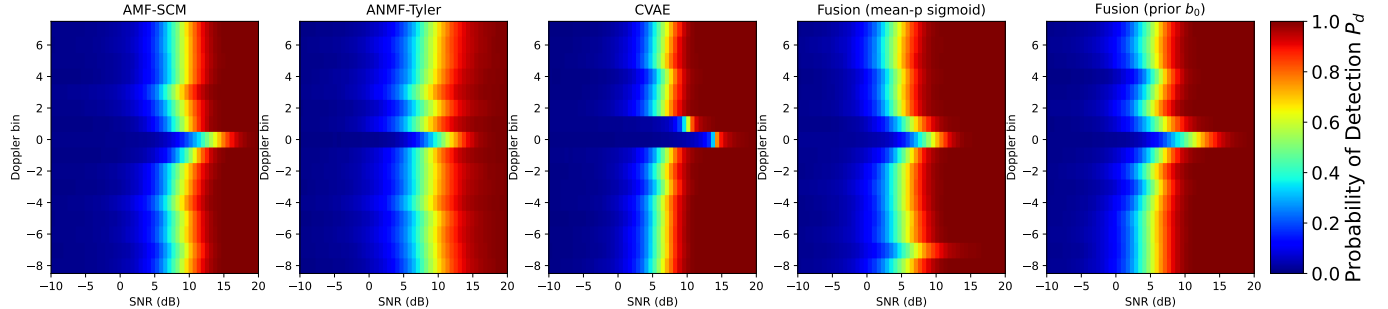


Fig. 9. P_d -SNR-Doppler maps for CFA16-008 (raw, $P_{fa} = 10^{-2}$). Left to right: AMF-SCM, ANMF-Tyler, CVAE, and proposed fusion (mean- p sigmoid and b_0 -prior variants).

On CFA16-008 with raw clutter (Fig. 9), AMF-SCM and ANMF-Tyler yield vertical SNR transition bands, with ANMF

slightly better near the clutter ridge ($d \approx 0$). The CVAE achieves a given P_d at lower SNR on most Doppler bins,

Fig. 10. P_d -SNR-Doppler maps for CFA16-008 (locally whitened).Fig. 11. P_d -SNR-Doppler maps for CFA16-002 (raw).Fig. 12. P_d -SNR-Doppler maps for CFA16-002 (locally whitened).

especially off clutter ridge ($|d| \geq 2$), and the fusion maps exploit this complementarity by tracking CVAE off clutter ridge while staying close to ANMF around $d \in \{-1, 0\}$. After whitening (Fig. 10), the CVAE fronts become more symmetric and shift further left, so that the CVAE dominates the parametric detectors on almost all bins, and the fused detector provides a smooth, high- P_d plateau across Doppler.

For CFA16-002 (Figs. 11–12), the absolute SNR levels change but the qualitative picture is similar: AMF-SCM and ANMF-Tyler show nearly vertical bands with moderate Doppler dependence, the CVAE improves detection on most bins (in particular off clutter ridge), and the fusion acts as an envelope of ANMF and CVAE, closing the small gap at central Doppler while preserving CVAE gains elsewhere. Whitening further homogenizes the maps and smooths the CVAE transitions, notably at low SNR. The qualitative Doppler-central vs. off clutter ridge behavior is summarized in Table III.

VI. CONCLUSION

We have proposed a complex-valued variational autoencoder for radar detection in non-Gaussian clutter, together with a decision-level fusion rule that combines its output with a model-based ANMF detector. The CVAE is trained only on clutter profiles under H_0 and used as an unsupervised generative model; detection relies on a complex reconstruction-error score, calibrated via per-Doppler probability-integral transforms to enforce CFAR. A local whitening scheme was also introduced to stabilize the covariance structure seen by the CVAE and reduce Doppler-wise variability in the null distribution of its scores.

On simulated correlated Gaussian and compound-Gaussian clutter, with and without additional white noise, the CVAE (especially with oracle whitening) closely tracks the MF/NMF baseline in nearly Gaussian regimes and significantly outperforms AMF-SCM and ANMF-Tyler in heavy-tailed or mixed scenarios. These results show that a purely data-driven gener-

TABLE III

QUALITATIVE RANKING AT $d=0$ (CLUTTER RIDGE) ON CSIR SEA CLUTTER ($P_{fa} = 10^{-2}$). SYMBOLS AS IN TABLE II. THESE RANKINGS ARE RESTRICTED TO THE CENTRAL DOPPLER BIN; OFF CLUTTER RIDGE ($|d| \geq 2$) THE CVAE AND THE PROPOSED FUSION GENERALLY DOMINATE ANMF-TYLER, AS SEEN IN FIGS. 9–12.

Scene / preprocessing	AMF-SCM	ANMF-Tyler	CVAE	Fusion (sigmoid)	Fusion (b_0 -prior)
CFA16-002, raw	+	++	–	+	++
CFA16-002, whitened	0	+	0	++	+
CFA16-008, raw	+	++	–	0	+
CFA16-008, whitened	+	+	+	++	+

ative model can recover matched-filter performance when the clutter model is well specified, while offering clear robustness gains when texture and correlation depart from the Gaussian paradigm. On real CSIR sea clutter, the CVAE alone is not uniformly superior to ANMF-Tyler on the clutter ridge, but achieves better detection on most other Doppler bins, particularly after local whitening. The proposed weighted log- p fusion exploits this complementarity: it takes advantage of both detectors namely ANMF-Tyler and CVAE, yielding smoother and more homogeneous P_d surfaces in the Doppler-SNR map while consistently respecting the designed CFAR level.

More broadly, our results illustrate that CVAEs, local covariance normalization, and calibrated p -value fusion can be combined to address out-of-distribution detection in non-Gaussian complex-valued signals. Promising extensions include moving from one-dimensional Doppler profiles to two-dimensional range-Doppler patches or multi-channel arrays, learning Doppler-dependent fusion weights directly from data while preserving CFAR, and enabling online adaptation of both the CVAE and the null calibration to slowly varying background conditions. Overall, the combination of a complex-valued VAE with classical ANMF through calibrated log- p fusion offers a flexible way to blend model-based and data-driven detection in challenging clutter environments with rigorous false-alarm rate control.

ACKNOWLEDGMENTS

Part of this work was supported by ANR-ASTRID NEPTUNE 3 (ANR-23-ASM2-0009).

REFERENCES

- [1] M. S. Greco and A. De Maio, Eds., *Modern Radar Detection Theory*. SciTech Publishing, Jan 2016.
- [2] F. C. Robey, D. R. Fuhrmann, E. J. Kelly, and R. Nitzberg, “A CFAR adaptive matched filter detector,” *IEEE Transactions on Aerospace and Electronic Systems*, vol. 28, pp. 208–216, 1992.
- [3] E. J. Kelly, “An adaptive detection algorithm,” *IEEE Transactions on Aerospace and Electronic Systems*, vol. AES-22, no. 2, pp. 115–127, 1986.
- [4] L. L. Scharf and B. Friedlander, “Matched subspace detectors,” *IEEE Transactions on Signal Processing*, vol. 42, no. 8, pp. 2146–2157, 1994.
- [5] I. J. Goodfellow, Y. Bengio, and A. Courville, *Deep Learning*. Cambridge, MA, USA: MIT Press, 2016.
- [6] X. Ran, M. Xu, L. Mei, Q. Xu, and Q. Liu, “Detecting Out-of-Distribution samples via Variational Auto-Encoder with reliable uncertainty estimation,” *Neural Networks*, vol. 145, pp. 199–208, 2022.
- [7] J. Yang, K. Zhou, Y. Li, and Z. Liu, “Generalized out-of-distribution detection: A survey,” *International Journal of Computer Vision*, Jun 2024.
- [8] D. P. Kingma and M. Welling, “An introduction to variational autoencoders,” *Foundations and Trends® in Machine Learning*, vol. 12, no. 4, p. 307–392, 2019.
- [9] M. Muzeau, C. Ren, S. Angelliaume, M. Datcu, and J.-P. Ovarlez, “Self-supervised learning based anomaly detection in Synthetic Aperture Radar imaging,” *IEEE Open Journal of Signal Processing*, vol. 3, pp. 440–449, 2022.
- [10] Z. Bukhsh and A. Saeed, “On out-of-distribution detection for audio with deep nearest neighbors,” in *IEEE International Conference on Acoustics, Speech and Signal Processing (ICASSP)*, 2023, pp. 1–5.
- [11] S. N. Marimont and G. Tarroni, “Anomaly detection through latent space restoration using vector quantized variational autoencoders,” in *IEEE 18th International Symposium on Biomedical Imaging (ISBI)*, 2021, pp. 1764–1767.
- [12] I. Mitiche, A. Salimy, F. Werner, P. Boreham, A. Nesbitt, and G. Morrison, “OODCN: Out-of-distribution detection in capsule networks for fault identification,” in *29th European Signal Processing Conference (EUSIPCO)*, 2021, pp. 1686–1690.
- [13] S. M. Kahya, M. S. Yavuz, and E. Steinbach, “MCROOD: Multi-class radar out-of-distribution detection,” in *IEEE International Conference on Acoustics, Speech and Signal Processing (ICASSP)*, 2023, pp. 1–5.
- [14] Y. A. Rouzoumka, E. Terreaux, C. Morisseau, J.-P. Ovarlez, and C. Ren, “Complex-Valued Variational Autoencoders for Radar Detection in Joint Compound Gaussian Clutter and Thermal Noise,” in *EUSIPCO 2025 - European Signal Processing Conference*, Palerme, Italy, Sep. 2025.
- [15] J. Fix, Q. Gabot, X. Huy N., J. Frontera-Pons, C. Ren, and J.-P. Ovarlez, “Torchcvnn: A PyTorch-based library to easily experiment with state-of-the-art Complex-Valued Neural Networks,” in *International Joint Conference on Neural Networks*, Rome, Italy, Jun. 2025.
- [16] J. A. Barrachina, C. Ren, C. Morisseau, G. Vieillard, and J.-P. Ovarlez, “Comparison Between Equivalent Architectures of Complex-valued and Real-valued Neural Networks - Application on Polarimetric SAR Image Segmentation,” *Journal of Signal Processing Systems*, Jul. 2022.
- [17] Y. Xie, T. Arildsen, and Z.-H. Tan, “Complex recurrent variational autoencoder for speech resynthesis and enhancement,” in *International Joint Conference on Neural Networks (IJCNN)*, 2024, pp. 1–7.
- [18] Y. Xiang, J. Tian, X. Hu, X. Xu, and Z. Yin, “A deep representation learning-based speech enhancement method using complex convolution recurrent variational autoencoder,” in *IEEE International Conference on Acoustics, Speech and Signal Processing (ICASSP)*, 2024, pp. 781–785.
- [19] R. A. Fisher, *Statistical Methods for Research Workers*, 4th ed. Edinburgh: Oliver and Boyd, 1932.
- [20] H. O. Lancaster, “The combination of probabilities: An application of orthonormal functions,” *Australian Journal of Statistics*, vol. 3, no. 1, pp. 20–33, 1961.
- [21] H. J. de Wind, J. E. Cilliers, and P. L. Herselman, “Dataware: Sea clutter and small boat radar reflectivity databases,” *IEEE Signal Processing Magazine*, vol. 27, no. 2, pp. 145–148, 2010.
- [22] P. L. Herselman and C. J. Baker, “Analysis of calibrated sea clutter and boat reflectivity data at c- and x-band in south african coastal waters,” in *IET International Conference on Radar Systems*, 2007, 2007.
- [23] N. Liu, X. Jiang, H. Ding, and Y. Xu, “Wave height inversion and sea state classification based on deep learning of radar sea clutter data,” *IEEE Geoscience and Remote Sensing Letters*, 2021.
- [24] L. Ma, J. Wu, J. Zhang, Z. Wu, and G. Jeon, “Research on sea clutter reflectivity using deep learning model in industry 4.0,” *IEEE Access*, vol. 7, pp. 171 652–171 662, 2019.
- [25] J. Gong, A. Wang, and W. Chen, “Lightcnn: A compact cnn for moving maritime targets detection,” in *IEEE Radar Conference*, 2020.
- [26] H. Ding, N. Liu, W. Zhou, Y. Xue, and J. Guan, “Construction of marine target detection dataset for intelligent radar application,” in *International Conference on Intelligent Computing*, 2020, pp. 333–344.

- [27] J. Tan, W. Sheng, and H. Zhu, "A sea clutter suppression method with graph neural network for maritime target detection," *IEEE Transactions on Aerospace and Electronic Systems*, 2025, early Access.
- [28] R. K. Kandagatla, V. Malapati, and K. Cherukuri, "Sea clutter suppression using neural network," *Marine Technology Research*, 2025.
- [29] S. Kraut, L. L. Scharf, and L. T. McWhorter, "Adaptive subspace detectors," *IEEE Transactions on Signal Processing*, vol. 49, pp. 1–16, 2001.
- [30] D. E. Tyler, "A distribution-free M-estimator of multivariate scatter," *Ann. Statist.*, vol. 15, no. 1, pp. 234–251, 03 1987.
- [31] F. Pascal, Y. Chitour, J.-P. Ovarlez, P. Forster, and P. Larzabal, "Covariance structure maximum-likelihood estimates in compound Gaussian noise: Existence and algorithm analysis," *IEEE Transactions on Signal Processing*, vol. 56, pp. 34–48, January 2008.
- [32] E. Ollila, D. E. Tyler, V. Koivunen, and H. V. Poor, "Complex elliptically symmetric distributions: Survey, new results and applications," *IEEE Transactions on Signal Processing*, vol. 60, no. 11, pp. 5597–5625, 2012.
- [33] J.-P. Ovarlez, F. Pascal, and A. Breloy, "Asymptotic detection performance analysis of the robust Adaptive Normalized Matched Filter," in *IEEE 6th International Workshop on Computational Advances in Multi-Sensor Adaptive Processing (CAMSAP)*, 2015, pp. 137–140.
- [34] F. Pascal, P. Forster, J.-P. Ovarlez, and P. Larzabal, "Performance analysis of covariance matrix estimates in impulsive noise," *IEEE Transactions on Signal Processing*, vol. 56, no. 6, pp. 2206–2217, 2008.
- [35] J. Neyman and E. S. Pearson, "On the problem of the most efficient tests of statistical hypotheses," *Philosophical Transactions of the Royal Society of London. Series A*, vol. 231, pp. 289–337, 1933.
- [36] Y. A. Rouzoumka, E. Terreaux, C. Morisseau, J.-P. Ovarlez, and C. Ren, "Out-of-distribution radar detection in compound clutter and thermal noise through variational autoencoders," in *IEEE International Conference on Acoustics, Speech and Signal Processing (ICASSP)*, 2025.
- [37] C. Baur, S. Denner, B. Wiestler, N. Navab, and S. Albarqouni, "Autoencoders for unsupervised anomaly segmentation in brain MR images: A comparative study," *Medical Image Analysis*, vol. 69, p. 101952, 2021.
- [38] H. Wu, J. Köhler, and F. Noe, "Stochastic normalizing flows," in *Advances in Neural Information Processing Systems*, H. Larochelle, M. Ranzato, R. Hadsell, M. F. Balcan, and H. Lin, Eds., vol. 33. Curran Associates, Inc., 2020, pp. 5933–5944.
- [39] D. Nielsen, P. Jaini, E. Hoogeboom, O. Winther, and M. Welling, "SurVAE flows: Surjections to bridge the gap between VAEs and flows," in *Advances in Neural Information Processing Systems*, H. Larochelle, M. Ranzato, R. Hadsell, M. Balcan, and H. Lin, Eds., vol. 33. Curran Associates, Inc., 2020, pp. 12 685–12 696.
- [40] W. Liu, X. Wang, J. Owens, and Y. Li, "Energy-based out-of-distribution detection," in *Advances in Neural Information Processing Systems*, H. Larochelle, M. Ranzato, R. Hadsell, M. F. Balcan, and H. Lin, Eds., vol. 33. Curran Associates, Inc., 2020, pp. 21 464–21 475.
- [41] W. Zhou, F. Liu, and M. Chen, "Contrastive out-of-distribution detection for pretrained transformers," in *Proceedings of the 2021 Conference on Empirical Methods in Natural Language Processing*. Association for Computational Linguistics, Nov. 2021, pp. 1100–1111.
- [42] X. Li, C. Desrosiers, and X. Liu, "Symmetric contrastive loss for out-of-distribution skin lesion detection," in *2022 IEEE 19th International Symposium on Biomedical Imaging (ISBI)*, 2022, pp. 1–5.
- [43] M. S. Graham, P.-D. Tudosiu, P. Wright, W. H. L. Pinaya, J.-M. U-King-Im, Y. H. Mah, J. T. Teo, R. Jager, D. Werring, P. Nachev, S. Ourselin, and M. J. Cardoso, "Transformer-based out-of-distribution detection for clinically safe segmentation," in *Proceedings of The 5th International Conference on Medical Imaging with Deep Learning*, ser. Proceedings of Machine Learning Research, vol. 172. PMLR, 06–08 Jul 2022, pp. 457–476.
- [44] J. Xu, H. Wu, J. Wang, and M. Long, "Anomaly transformer: Time series anomaly detection with association discrepancy," *ArXiv*, vol. abs/2110.02642, 2021.
- [45] S. Tuli, G. Casale, and N. R. Jennings, "TranAD: Deep Transformer Networks for Anomaly Detection in Multivariate Time Series Data," *Proceedings of VLDB*, vol. 15, no. 6, pp. 1201–1214, 2022.
- [46] S. M. Kahya, M. S. Yavuz, and E. Steinbach, "HOOD: Real-time human presence and out-of-distribution detection using FMCW radar," *IEEE Transactions on Radar Systems*, vol. 3, pp. 44–56, 2025.
- [47] T. Nakashika, "Complex-valued variational autoencoder: A novel deep generative model for direct representation of complex spectra," in *Interspeech 2020*, 2020, pp. 2002–2006.
- [48] D. P. Kingma and M. Welling, "Auto-encoding variational Bayes," in *2nd International Conference on Learning Representations, ICLR*, 2014.
- [49] B. Picinbono, "Second-order complex random vectors and Normal distributions," *IEEE Transactions on Signal Processing*, vol. 44, no. 10, pp. 2637–2640, 1996.
- [50] P. J. Schreier and L. L. Scharf, *Statistical Signal Processing of Complex-Valued Data: The Theory of Improper and Noncircular Signals*. Cambridge University Press, 2010.
- [51] O. Ledoit and M. Wolf, "A well-conditioned estimator for large-dimensional covariance matrices," *Journal of Multivariate Analysis*, vol. 88, no. 2, pp. 365–411, 2004.
- [52] M. Rosenblatt, "Remarks on a Multivariate Transformation," *The Annals of Mathematical Statistics*, vol. 23, no. 3, pp. 470 – 472, 1952.
- [53] F. X. Diebold, T. A. Gunther, and A. S. Tay, "Evaluating density forecasts with applications to financial risk management," *International Economic Review*, vol. 39, no. 4, pp. 863–883, 1998.
- [54] T. Gneiting and A. E. Raftery, "Strictly proper scoring rules, prediction, and estimation," *Journal of the American Statistical Association*, vol. 102, no. 477, pp. 359–378, 2007.
- [55] P. Massart, "The tight constant in the Dvoretzky-Kiefer-Wolfowitz inequality," *The Annals of Probability*, vol. 18, no. 3, pp. 1269–1283, 1990.